Damping Rotating Grid SINS Based on a Kalman Filter for Shipborne Application

TAO FANG[ID], WEIQUAN HUANG, AND LI LUO
College of Automation, Harbin Engineering University, Harbin 150001, China
Corresponding author: Weiquan Huang (huangweiquan@hrbeu.edu.cn)

ABSTRACT The measurement error of the inertial measurement unit (IMU) significantly affects the navigation accuracy of the grid strap-down inertial navigation system (SINS) applied in polar regions. In this paper, the single-axis rotation modulation grid SINS is designed to suppress the navigation error caused by IMU constant error. Then on the basis of rotation modulation scheme, a novel external horizontal damping algorithm based on a Kalman filter is conducted to further suppress the 84.4 min Schuler oscillation caused by IMU random error. The Kalman filter is established based on the error model of shipborne grid SINS. When the reference velocity provided by Doppler velocity log is usable, the Schuler oscillation can be restrained through feedback calibration by calibrating the grid horizontal attitude errors and grid horizontal velocity errors. The simulation results demonstrate that the proposed external horizontal damping algorithm can efficiently suppress the Schuler oscillation, meanwhile compared with traditional external horizontal damping algorithm based on damping network, the proposed algorithm has the advantage of reducing the overshoot errors in the process of state switching.

INDEX TERMS External horizontal damping, grid SINS, Kalman filter, rotation modulation.

I. INTRODUCTION

Navigating in polar regions reliably and safely is an important ability for modern ships [1], [2]. Strap-down inertial navigation system (SINS) has become the core navigation system for ships navigating in polar regions due to its particular advantages, such as autonomy, continuity, and completeness [3], [4]. The frequently-used north-pointing SINS mechanization has the problems of overflow and error magnification when calculating the relevant parameters in high-latitude areas [5]–[7]. The free azimuth SINS mechanization and the wander azimuth SINS mechanization can overcome the problems of overflow and error magnification. But there is singular value when extracting the position from the position direction cosine matrix in high-latitude areas [8]. The grid SINS mechanization and the transversal SINS mechanization can solve the problems of abovementioned mechanizations [9]–[12]. The problems such as overflow, error magnification, and singular value phenomenon do not exist in the transversal SINS mechanization, but the earth is assumed to be a standard sphere in the conversion process from the earth-centered earth-fixed (ECEF) frame to the transversal frame. In this way, the theoretical error is introduced to the transversal SINS mechanization [13], [14].

Grid SINS mechanization does not have theoretical error, so it can be the best choice for SINS working in polar regions [15].

The measurement error of the inertial measurement unit (IMU) is the main error source for the error accumulation of grid SINS [16], [17]. Consequently, in order to ensure that the navigation accuracy meets the requirements of ships navigating in polar regions, some measures must be conducted to suppress the navigation error caused by IMU measurement error. The rotation modulation technique can effectively restrain the navigation error caused by IMU constant error. However, the rotation modulation technique cannot restrain the navigation error caused by IMU random error [18]. So when the rotation modulation technique is conducted to improve the navigation accuracy of grid SINS, the navigation error caused by IMU random error tends to be the main error in the system.

The rotation modulation technique does not change the non-damping essence of the system. The navigation error of the single-axis rotation modulation grid SINS mainly manifests as three kinds of oscillations: the 84.4 min Schuler oscillation, the Foucault oscillation, and the 24 h Earth oscillation [19], [20]. Aiming at the ship which has reference information to perform system reset termly, damping the

Schuler oscillation can further improve the navigation accuracy of the single-axis rotation modulation grid SINS. The external horizontal damping technique is an effective way to suppress the Schuler oscillation. The pure external horizontal damping technique cannot completely restrain the navigation error caused by IMU measurement error. For example, the attitude errors caused by accelerometer constant bias still exist in the system, and the position accuracy cannot meet the requirements of a long-endurance SINS [21]. Therefore, the combination of rotation modulation technique and damping technique can be the suitable way to improve the navigation accuracy of grid SINS.

External horizontal damping state and non-damping state are two common states of the system, thus the system state frequently switches between these two states [22]. The traditional external horizontal damping technique damps the Schuler oscillation by introducing the external velocity to the horizontal circuit through the damping network. However, the traditional network-based damping method brings the overshoot errors to the system when the system state switches from non-damping state to damping state, and the overshoot errors will lead to the degradation of the navigation accuracy in the process of state switching [23]. With regard to the overshoot errors caused by the switch, an adaptive damping network was adopted in [22]. The jump in damping coefficient was transformed into gradual change to reduce the overshoot errors. However, each damping coefficient requires to design a different damping network, which increases the complexity of designing the damping network, and the size of the acceleration needs to be obtained so as to get the parameters of the damping network. An automatic compensation method was adopted in [24]. In order to reduce the overshoot errors, the instantaneous velocity at switch moment is compensated to the damping network. However, the design process of the damping network is complicated and only a single damping network cannot adapt to the change of external velocity error. Reference [25] adopts the Kalman filter to realize the damping and reduce the overshoot errors. However, the error of speed measurement device is considered as white noise, and the method to reduce the overshoot errors is not mentioned. A generalized damping algorithm based on dual-model mean is adopted to suppress the Schuler oscillation as well as reduce the overshoot errors in [26]. However, two calculating loops are required.

The main contributions of the paper include the following two aspects: (1) the single-axis rotation modulation grid SINS is designed to restrain the navigation error caused by IMU constant error; (2) in order to further improve the navigation accuracy of the single-axis rotation modulation grid SINS, aiming at the overshoot errors in the process of state switching, a novel external horizontal damping algorithm based on a Kalman filter is proposed to suppress the Schuler oscillation as well as reduce the overshoot errors in the process of state switching. The single-axis rotation modulation grid SINS/DVL integrated Kalman filter is established based on shipborne grid SINS error model. When the velocity

measured by DVL is available, the grid horizontal attitude errors and grid horizontal velocity errors can be estimated accurately. Compensating the grid horizontal attitude errors and grid horizontal velocity errors through feedback calibration can improve the navigation accuracy effectively. Simulation results demonstrate that the proposed damping algorithm can efficiently suppress the Schuler oscillation, meanwhile it has the advantage of reducing the overshoot errors in the process of state switching. In the following paper, GSINS represents the grid SINS; RMGSINS represents the single-axis rotation modulation grid SINS; T-RMGSINS represents the single-axis rotation modulation grid SINS which conducts the traditional external horizontal damping algorithm; KF-RMGSINS represents the single-axis rotation modulation grid SINS which conducts the proposed external horizontal damping algorithm.

II. RMGSINS

This section first introduces the GSINS mechanization, then the principle of the single-axis rotation modulation technique is introduced. The common coordinate systems used in this paper include:

ECEF frame — e;
Body frame — b;
Geographic frame — g;
Geocentric inertial frame — i;
Rotating frame — p;
Grid frame — G;
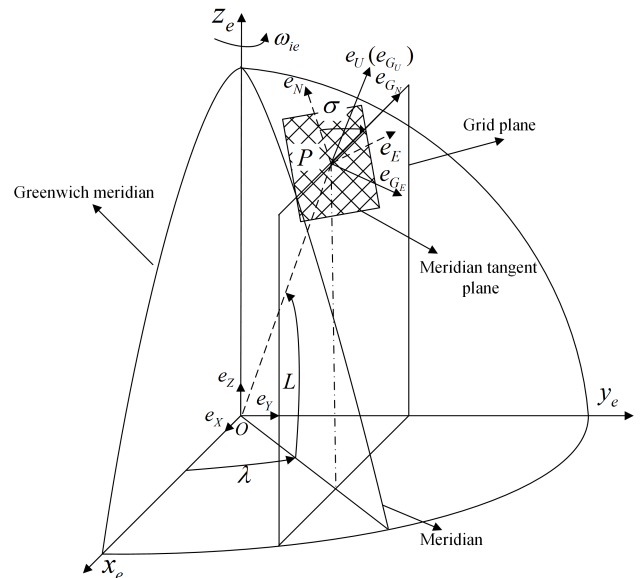The grid frame is shown in Fig. 1.

FIGURE 1. The grid frame.

As shown in the figure, the ship locates on point P. The grid plane is parallel to the Greenwich plane which passes through P; the meridian tangent plane is the local horizontal plane which passed through P. The grid frame is defined

as follows: the grid north axis G_N is the intersecting line of the meridian tangent plane and grid plane; the grid up axis G_U is perpendicular to the horizontal plane which passes through P; the grid east axis G_E lies in the horizontal plane and is perpendicular to G_N. G_E, G_N and G_U constitute the right-handed coordinate system.

The definitions of the frames can refer to [27] and [28].

A. GSINS MECHANIZATION

The grid frame is chosen as the navigation frame. The gyroscopes and the accelerometers are strapped on the carrier. The gyroscopes measure the angular motion of the carrier, and the accelerometers measure the linear motion of the carrier. The navigation computer calculates the position, the velocity, and the attitude of the carrier based on the grid SINS mechanization with the outputs of gyroscopes and accelerometers. The attitude differential equation is described as follow:

$$\dot{C}_b^G = C_b^G \left[\omega_{Gb}^b \times \right] = C_b^G \left\{ \left[\omega_{ib}^b - C_G^b (\omega_{ie}^G + \omega_{eG}^G) \right] \times \right\} \quad (1)$$

where ω_{ib}^b represents the output of the gyroscope, and ω_{ie}^G can be calculated as follow:

$$
\begin{aligned}
\omega_{ie}^G &= C_g^G \omega_{ie}^g \\
&= \begin{bmatrix} \cos\sigma & -\sin\sigma & 0 \\ \sin\sigma & \cos\sigma & 0 \\ 0 & 0 & 1 \end{bmatrix} \begin{bmatrix} 0 \\ \omega_{ie}\cos L \\ \omega_{ie}\sin L \end{bmatrix} \\
&= \begin{bmatrix} -\omega_{ie}\cos L\sin\sigma \\ \omega_{ie}\cos L\cos\sigma \\ \omega_{ie}\sin L \end{bmatrix}
\end{aligned} \quad (2)
$$

where ω_{ie} is the rotational angular velocity constant of the earth, and σ represents the included angle of the geographic north and the grid north.

ω_{eG}^G can be calculated as follow:

$$
\omega_{eG}^G = \begin{bmatrix} \dfrac{1}{\tau_{fG}} & -\dfrac{1}{R_{yG}} \\[2mm] \dfrac{1}{R_{xG}} & -\dfrac{1}{\tau_{fG}} \\[2mm] \dfrac{\kappa_G}{\tau_{fG}} & -\dfrac{\kappa_G}{R_{yG}} \end{bmatrix} \begin{bmatrix} V_{GE} \\ V_{GN} \end{bmatrix} \quad (3)
$$

where V_{GE} and V_{GN} represent the grid east velocity and the grid north velocity of the ship; $\frac{1}{\tau_{fG}}$, $\frac{1}{R_{xG}}$, $\frac{1}{R_{yG}}$, and κ_G can be calculated as follows:

$$
\begin{cases}
\dfrac{1}{\tau_{fG}} = (\dfrac{1}{R_M} - \dfrac{1}{R_N})\sin\sigma\cos\sigma \\[2mm]
\dfrac{1}{R_{xG}} = \dfrac{\sin^2\sigma}{R_M} + \dfrac{\cos^2\sigma}{R_N} \\[2mm]
\dfrac{1}{R_{yG}} = \dfrac{\sin^2\sigma}{R_N} + \dfrac{\cos^2\sigma}{R_M} \\[2mm]
\kappa_G = \dfrac{\cos L\sin\lambda}{\sqrt{1 - \cos^2 L\sin^2\lambda}}
\end{cases} \quad (4)
$$

where λ and L represent the longitude and the latitude of the ship; R_M and R_N represent the radiuses of curvature in meridian and prime vertical.

The velocity differential equation is described as follow:

$$\dot{V}^G = C_b^G f^b - (2C_g^G \omega_{ie}^g + \omega_{eG}^G) \times V^G + g^G \quad (5)$$

where f^b represents the output of the accelerometer. $g^G = \begin{bmatrix} 0 & 0 & -g \end{bmatrix}^T$, and g is the gravitational acceleration.

The position differential equation is described as follow:

$$\dot{R}^e = C_G^e V^G \quad (6)$$

where $R^e = \begin{bmatrix} x & y & z \end{bmatrix}^T$, and the transpose of C_G^e can be calculated as follow:

$$
\begin{aligned}
C_e^G &= C_g^G C_e^g \\
&= \begin{bmatrix} \cos\sigma & -\sin\sigma & 0 \\ \sin\sigma & \cos\sigma & 0 \\ 0 & 0 & 1 \end{bmatrix} \\
&\quad \times \begin{bmatrix} -\sin\lambda & \cos\lambda & 0 \\ -\sin L\cos\lambda & -\sin L\sin\lambda & \cos L \\ \cos L\cos\lambda & \cos L\sin\lambda & \sin L \end{bmatrix}
\end{aligned} \quad (7)
$$

The sine and the cosine of σ can be calculated as follows:

$$
\begin{cases}
\sin\sigma = \dfrac{\sin L\sin\lambda}{\sqrt{1 - \cos^2 L\sin^2\lambda}} \\[3mm]
\cos\sigma = \dfrac{\cos\lambda}{\sqrt{1 - \cos^2 L\sin^2\lambda}}
\end{cases} \quad (8)
$$

B. THE PRINCIPLE OF THE SINGLE-AXIS ROTATION MODULATION TECHNIQUE

The rotation mechanism and the angle measuring device are introduced to RMGSINS. IMU is strapped with the rotation mechanism, and IMU does the periodic rotation about the rotation axis with the rotation mechanism. In this paper, the sensing axis of the up gyroscope is taken as the rotation axis, and the frequently-used positive and negative continuous rotation scheme is chosen as the rotation scheme.

IMU rotating frame coincides with body frame at the initial moment. IMU rotating frame rotates about the rotation axis with the constant angular velocity Ω. The included angle between IMU rotating frame and body frame is expressed as Ωt. The transformation matrix between IMU rotating frame and body frame is described as follow:

$$
C_b^p = \begin{bmatrix} \cos\Omega t & \sin\Omega t & 0 \\ -\sin\Omega t & \cos\Omega t & 0 \\ 0 & 0 & 1 \end{bmatrix} \quad (9)
$$

In RMGSINS, the outputs of the gyroscope and the accelerometer are expressed as ω_{ip}^p and f_{ip}^p. In order to perform the navigation solution, the IMU outputs should be transformed from IMU rotating frame to body frame which can be realized as follows:

$$
\begin{cases}
\omega_{ib}^b = (C_b^p)^T \omega_{ip}^p + \omega_{pb}^b \\
f_{ib}^b = (C_b^p)^T f_{ip}^p + f_{pb}^b
\end{cases} \quad (10)
$$

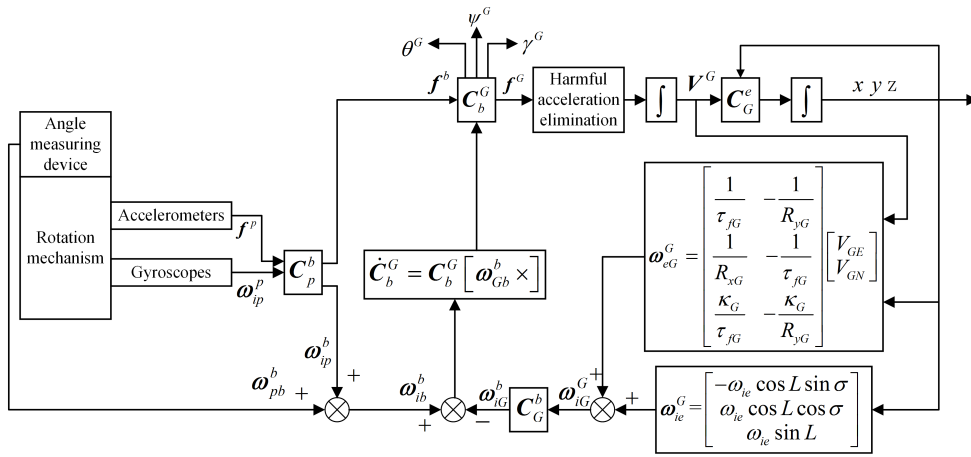where $\omega_{pb}^b = \begin{bmatrix} 0 & 0 & -\Omega \end{bmatrix}^T$ and $f_{pb}^b = \mathbf{0}$.

FIGURE 2. Block diagram of RMGSINS mechanization.

The IMU outputs within IMU rotating frame can be described as follows:

$$\begin{cases} \boldsymbol{\omega}_{ip}^p = \boldsymbol{C}_b^p \boldsymbol{\omega}_{ib\_true}^b + \begin{bmatrix} \varepsilon_x & \varepsilon_y & \varepsilon_z \end{bmatrix}^T + \boldsymbol{\omega}_{bp}^p \\ \boldsymbol{f}_{ip}^p = \boldsymbol{C}_b^p \boldsymbol{f}_{ib\_true}^b + \begin{bmatrix} \nabla_x & \nabla_y & \nabla_z \end{bmatrix}^T + \boldsymbol{f}_{bp}^p \end{cases} \quad (11)$$

where $\boldsymbol{\omega}_{ib\_true}^b$ and $\boldsymbol{f}_{ib\_true}^b$ represent the ideal IMU outputs with no measurement errors. ε_x, ε_y, and ε_z represent the gyroscope drifts along the x, y, and z axes of IMU rotating frame; ∇_x, ∇_y, and ∇_z represent the accelerometer biases along the x, y, and z axes of IMU rotating frame. $\boldsymbol{\omega}_{bp}^p = \begin{bmatrix} 0 & 0 & \Omega \end{bmatrix}^T$ and $\boldsymbol{f}_{bp}^p = \boldsymbol{0}$.

By substituting (11) into (10), $\boldsymbol{\omega}_{ib}^b$ and $\boldsymbol{f}_{ib}^b$ can be expressed as follows:

$$\begin{cases} \begin{bmatrix} \omega_{ibx}^b \\ \omega_{iby}^b \\ \omega_{ibz}^b \end{bmatrix} = \boldsymbol{\omega}_{ib\_true}^b + \begin{bmatrix} \varepsilon_x \cos \Omega t - \varepsilon_y \sin \Omega t \\ \varepsilon_x \sin \Omega t + \varepsilon_y \cos \Omega t \\ \varepsilon_z \end{bmatrix} \\ \begin{bmatrix} f_{ibx}^b \\ f_{iby}^b \\ f_{ibz}^b \end{bmatrix} = \boldsymbol{f}_{ib\_true}^b + \begin{bmatrix} \nabla_x \cos \Omega t - \nabla_y \sin \Omega t \\ \nabla_x \sin \Omega t + \nabla_y \cos \Omega t \\ \nabla_z \end{bmatrix} \end{cases} \quad (12)$$

As shown in (12), the IMU constant errors along the x and y axes of IMU rotating frame have been modulated as the form of periodic change. After the integrating process in a complete period, the navigation error caused by IMU constant errors along the x and y axes can be eliminated. However, the single-axis rotation modulation technique cannot modulate the IMU random error and the IMU constant error along the rotation axis, which means the IMU random error and the IMU constant error along the rotation axis will still lead to the degradation of navigation accuracy. The block diagram of RMGSINS mechanization is shown in Fig. 2. In Fig. 2, θ^G, ψ^G, and γ^G denote the grid pitch angle, grid yaw angle, and grid roll angle, respectively.

III. KF-RMGSINS
The error model of shipborne GSINS is introduced in this section first, next the criterion is deduced to judge whether the velocity provided by DVL is available, then the method to reduce the overshoot errors is given, finally the shortcomings of T-RMGSINS are expressed.
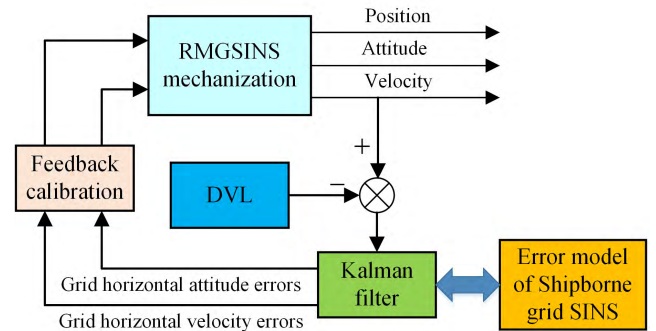
FIGURE 3. Schematic diagram of KF-RMGSINS.

Due to the included angles between grid frame and mathematical platform frame, the Schuler oscillation occurs under the system disturbances. The included angles are the so-called grid horizontal attitude error angles [27]. In this way, compensating the grid horizontal attitude error angles theoretically can suppress the Schuler oscillation. The schematic diagram of KF-RMGSINS is shown in Fig. 3. When the velocity measured by DVL is available, due to the constant error of DVL, when there are no measures to compensate the DVL measurement error, only the estimates of the grid horizontal attitude errors and the grid horizontal velocity errors can be used to calibrate the system. Compensating the grid horizontal attitude errors and the grid horizontal velocity errors through feedback calibration can efficiently suppress the Schuler oscillation. Because the grid horizontal velocity errors are also compensated, compared with traditional

horizontal damping algorithm, the proposed KF-RMGSINS can achieve a higher navigation accuracy.

A. ERROR MODEL AND FEEDBACK CALIBRATION

The rotation modulation technique suppresses the IMU constant error without changing the error propagation rule of GSINS. Reference [7] has given the error model of the airborne GSINS. The altitude channel of the system needs to be ignored so as to make the model adapt to the shipborne application. The linear process equation and measurement model are expressed as follows:

$$\begin{cases} \dot{X} = AX + W \\ Z = HX + \eta \end{cases} \tag{13}$$

where $X = [\phi_{GE} \ \phi_{GN} \ \phi_{GU} \ \delta V_{GE} \ \delta V_{GN} \ \delta X \ \delta Y \ \delta Z \ \delta V_{rGE}$ $\delta V_{rGN}]^T$. ϕ_{GE}, ϕ_{GN}, and ϕ_{GU} represent the grid attitude errors; δV_{GE} and δV_{GN} represent the grid east velocity error and the grid north velocity error; δX, δY, and δZ represent the position errors within e frame; δV_{rGE} and δV_{rGN} represent the measurement errors of DVL along the grid east and the grid north. A represents the coefficient matrix; W represents the driving noise vector, $W \sim N(0, Q)$, and Q is the variance matrix of the driving noise vector; Z represents the observation of the filter; H represents the observation matrix; η represents the measurement noise array, $\eta \sim N(0, T)$, and T is the variance matrix of the external velocity measurement error. The detailed expressions of the coefficient matrix A and the observation matrix H are expressed as follows:

$$A = \begin{bmatrix} A_{11} & A_{12} & A_{13} & \vdots & 0_{8 \times 2} \\ A_{21} & A_{22} & A_{23} & \vdots & \\ A_{31} & A_{32} & A_{33} & \vdots & \\ \hdashline & & 0_{2 \times 10} & & \end{bmatrix} \tag{14}$$

where $A_{11} = -(\omega_{iG}^G \times)$, $A_{12} = (C_{\omega Gv})_{3,2}$, $A_{13} = C_{\omega eR} + C_{\omega GR}$, $A_{21} = (f^G \times)_{2,3}$, $A_{22} = (V^G \times C_{\omega Gv} - (2\omega_{ie}^G + \omega_{eG}^G) \times)_{2,2}$, $A_{23} = (V^G \times (C_{\omega GR} + 2C_{\omega eR}))_{2,3}$, $A_{31} = 0_{3 \times 3}$, $A_{32} = (C_G^e)_{3,2}$, and $A_{33} = -C_G^e (V^G \times) C_R$. $(vector \times)$ represents the skew-symmetric matrix related to $vector$, and $(matrix)_{m,n}$ represents the first m rows and the first n columns of the $matrix$. The detailed expressions of matrixes $C_{\omega Gv}$, $C_{\omega eR}$, $C_{\omega GR}$, and C_R are described in [7].

$$H = \begin{bmatrix} 0 & 0 & 0 & 1 & 0 & 0 & 0 & 0 & -1 & 0 \\ 0 & 0 & 0 & 0 & 1 & 0 & 0 & 0 & 0 & -1 \end{bmatrix} \tag{15}$$

The KF-RMGSINS is illustrated by the grid north channel of grid horizontal circuit, and its block diagram is shown in Fig. 4. In Fig. 4, s denotes the complex variable in complex frequency domain; R denotes the radius of the earth; $\hat{\phi}_{GE}$ denotes the grid east attitude error estimated by filter; $\delta \hat{V}_{GN}$ denotes the grid north velocity error estimated by filter. When the velocity measured by DVL is available, due to the constant error of DVL caused by ocean currents, only the estimates of the grid horizontal attitude errors and the grid horizontal velocity errors can be used to calibrate the system.

FIGURE 4. Block diagram of KF-RMGSINS.

The common calibration methods can be divided into the output calibration and the feedback calibration. Obviously, when the output calibration is conducted to compensate the system errors, only the grid horizontal attitude errors and the grid horizontal velocity errors can be suppressed, and the position error still drifts with time. However, when the feedback calibration is conducted to calibrate the system, the accuracy of the grid horizontal attitude angles and the grid horizontal velocities can be effectively improved. Meanwhile, due to the closed-loop essence of the system, the accuracy of the position can also be improved.

B. THE CRITERION OF THE STATE SWITCHING

In III-A, when the velocity measured by DVL is available, the velocity error model of DVL is established as a constant. The main reason is expressed as follows: when the ship sails on the sea, under most circumstances, the Doppler beam transmitted by DVL cannot reach the seafloor. Due to the ocean currents, the velocity measured by DVL usually contains the error caused by the ocean currents. However, establishing the accurate velocity model of the ocean currents is extremely difficult. In practical engineering application, the velocity of the ocean currents does not change in a certain period of time, thus the velocity of the ocean currents can be regarded as a constant. In this case, the error model of DVL can be established as the periodical constant. According to the availability of the external velocity measured by DVL, the system state frequently switches between horizontal damping state and non-damping state. When the velocity measured by DVL is available, RMGSINS navigates in damping state; otherwise RMGSINS navigates in non-damping state. Consequently, a practical criterion needs to be built to judge the availability of the DVL. The derivation of the criterion is described as follows:

$$\begin{cases} V_{RMGSINS} = V_{true} + \delta V_{RMGSINS} \\ V_{DVL} = V_{true} + \delta V_{DVL} \end{cases} \tag{16}$$

where $V_{RMGSINS}$ and V_{DVL} represent the velocities of RMGSINS and DVL, respectively; $\delta V_{RMGSINS}$ and δV_{DVL} represent the velocity errors of RMGSINS and DVL, respectively; V_{true} represents the theoretical true value of the velocity. The observations of the filter at time t_1 and its adjacent

time t_2 are calculated as follows:

$$\begin{cases} Z_{t_1} = V_{RMGSINS}^{t_1} - V_{DVL}^{t_1} = \delta V_{RMGSINS}^{t_1} - \delta V_{DVL}^{t_1} \\ Z_{t_2} = V_{RMGSINS}^{t_2} - V_{DVL}^{t_2} = \delta V_{RMGSINS}^{t_2} - \delta V_{DVL}^{t_2} \end{cases} \quad (17)$$

where Z_{t_1} and Z_{t_2} represent the observations at time t_1 and t_2, respectively. The difference between Z_{t_1} and Z_{t_2} can be calculated as follow:

$$\delta Z_{t_2 \to t_1} = Z_{t_2} - Z_{t_1} = (\delta V_{RMGSINS}^{t_2} - \delta V_{RMGSINS}^{t_1}) \\ - (\delta V_{DVL}^{t_2} - \delta V_{DVL}^{t_1}) \quad (18)$$

Due to the continuity of SINS, $(\delta V_{RMGSINS}^{t_2} - \delta V_{RMGSINS}^{t_1})$ will not change drastically within a short time. In this way, as long as $\delta Z_{t_2 \to t_1}$ changes drastically within a short time, which means the measurement error of DVL changes drastically, and the velocity measured by DVL cannot be used as the reference. Consequently, if the difference of the observations between two adjacent moments changes drastically, RMGSINS works in non-damping state; otherwise RMGSINS works in horizontal damping state.

C. THE SUPPRESSION OF OVERSHOOT ERRORS

In order to reduce the overshoot errors, the feedback calibration should start after the filter has worked in a steady state. In other words, the feedback calibration should start after the estimates of grid horizontal attitude errors and grid horizontal velocity errors are accurate.

When the error model is established accurately, the diagonal elements of error covariance matrix $\boldsymbol{P}_k$ indicate the estimation performance of the corresponding state variables, and the diagonal elements quantificationally describe the estimation performance of the state variables. Therefore the changing process of diagonal element indicates the change of estimation performance. Meanwhile, we can easily get a conclusion that the smaller diagonal element means the better estimation performance of the corresponding state variable. In this paper, a simulation test is conducted to determine the start time of the feedback calibration. The simulation time is set as 2 h, and the simulation conditions are set as Table 1:

TABLE 1. Simulation conditions.

Simulation parameter	Parameter value
accelerometer constant bias (g)	10^{-4}
gyroscope constant drift ($^\circ$/h)	0.01
initial latitude	85° N
initial longitude	18° E
IMU random error	white noise
angular rate of the rotation mechanism ($^\circ$/s)	10
initial grid pitch error (arc sec)	6
initial grid roll error (arc sec)	6
initial grid yaw error (arc min)	6

The ship sails along the $85^\circ N$ latitude circle with the velocity of 10 m/s. The measurement error of DVL is set as the sum of the constant (1 nmile) and white noise with
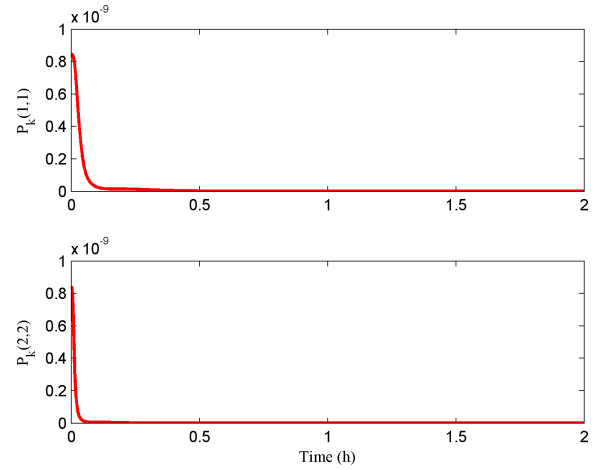
FIGURE 5. Estimation performance changing curves of ϕ_{GE} and ϕ_{GN}.

small amplitude so as to simulate the condition that the velocity measured by DVL is available. The swing maneuver condition is set as the following form:

$$\begin{cases} pitch = pitch_m \sin(\dfrac{2\pi}{T_p} t + \varphi_p) \\ roll = roll_m \sin(\dfrac{2\pi}{T_r} t + \varphi_r) \\ yaw = 90^\circ + yaw_m \sin(\dfrac{2\pi}{T_y} t + \varphi_y) \end{cases} \quad (19)$$

where the swing amplitudes $pitch_m = 3^\circ$, $roll_m = 5^\circ$, and $yaw_m = 0^\circ$; the swing periods $T_p = 3$ s, $T_r = 4$ s, and $T_y = 5$ s; the initial phases φ_p, φ_r, and φ_y are set as random value.

The diagonal elements $\boldsymbol{P}_k(1, 1)$, $\boldsymbol{P}_k(2, 2)$, $\boldsymbol{P}_k(4, 4)$, and $\boldsymbol{P}_k(5, 5)$ indicate the estimation performance of ϕ_{GE}, ϕ_{GN}, δV_{GE}, and δV_{GN}. The changing curves of $\boldsymbol{P}_k(1, 1)$, $\boldsymbol{P}_k(2, 2)$, $\boldsymbol{P}_k(4, 4)$, and $\boldsymbol{P}_k(5, 5)$ are shown in Fig. 5-Fig. 6.
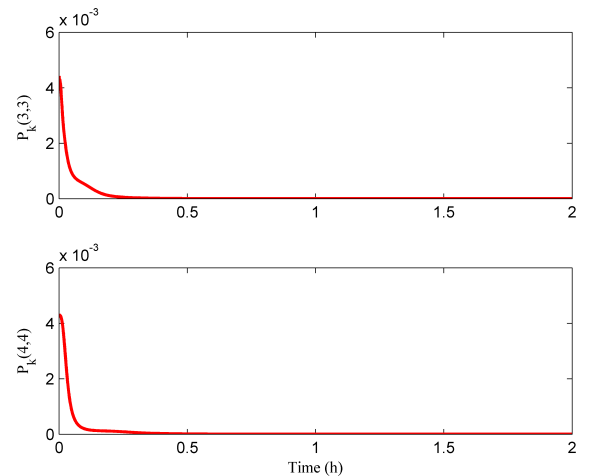

FIGURE 6. Estimation performance changing curves of δV_{GE} and δV_{GN}.

As shown in Fig. 5-Fig. 6, after about 0.2 h, the estimates of ϕ_{GE}, ϕ_{GN}, δV_{GE}, and δV_{GN} tend to be steady. In this

way, in order to reduce the overshoot errors, the feedback calibration should start after about 0.2 h.

D. THE SHORTCOMINGS OF T-RMGSINS

The introduction of the rotation mechanism will not change the horizontal circuit of the system. In this way, refer to the north-pointing SINS, T-RMGSINS can be designed. The traditional external horizontal damping algorithm damps the Schuler oscillation by introducing the external velocity to the grid horizontal circuit through the damping network. The detailed expression of horizontal damping network is expressed as follow:

$$H_y(s) = \frac{(s + 8.5 \times 10^{-4})(s + 9.412 \times 10^{-2})}{(s + 8.0 \times 10^{-3})(s + 1.0 \times 10^{-2})} \quad (20)$$

Take the grid north channel of horizontal circuit for instance. The block diagram of T-RMGSINS is shown in Fig. 7.
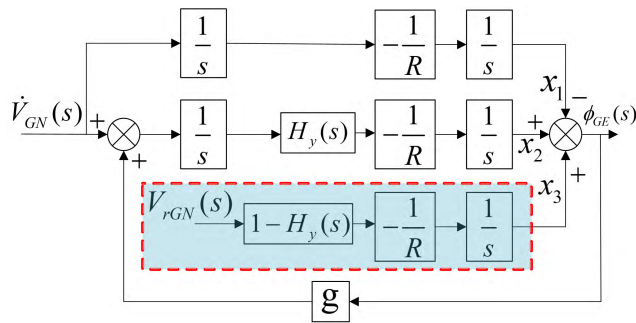
FIGURE 7. Block diagram of T-RMGSINS.

As shown in Fig. 7, the grid east attitude error $\phi_{GE}(s)$ can be calculated as follow:

$$\phi_{GE}(s) = x_2 + x_3 - x_1 \quad (21)$$

where x_1, x_2, and x_3 can be expressed as follows:

$$\begin{cases} x_1 = -\frac{1}{s^2 R}\dot{V}_{GN}(s) \\ x_2 = -\frac{H_y(s)}{s^2 R}[\dot{V}_{GN}(s) + g\phi_{GE}(s)] \\ x_3 = -\frac{1}{sR}[1 - H_y(s)]V_{rGN}(s) \end{cases} \quad (22)$$

The velocity measured by DVL can be described as follow:

$$V_{rGN}(s) = V_{GN}(s) + \delta V_{rGN}(s) \quad (23)$$

By substituting (22) and (23) into (21), the grid east attitude error $\phi_{GE}(s)$ can be described as another form:

$$\phi_{GE}(s) = \frac{[H_y(s) - 1]s}{R\left[s^2 + H_y(s)\frac{g}{R}\right]}\delta V_{rGN}(s) \quad (24)$$

As shown in (24), the velocity error of DVL will introduce the new error to the system. Time is needed for the system to reach the steady-state condition $H_y(s) \to 1$, in this way, when the velocity measured by DVL contains error, the external velocity error will introduce the new error to the system.

When the system state switches from non-damping state to damping state, this new error is the so-called "overshoot phenomenon." The shortcomings of T-RMGSINS can be summarized as follows:

1) The damping network can only be designed through the tried-and-tested rule, and only one damping network cannot adapt to the complex change of the sea conditions.
2) T-RMGSINS is designed based on the premise of the single input single output system, so it is hard to solve the problem of coupling effects between the grid east horizontal circuit and the grid north horizontal circuit.
3) The overshoot phenomenon occurs in the process of state switching, which results in navigation accuracy degradation of the system.

IV. RESULTS AND DISCUSSIONS

This section first introduces the simulation results and discussions, then the semi-physical simulation results and discussions are introduced.

A. SIMULATION RESULTS AND DISCUSSIONS

The single-axis rotation modulation technique can suppress the navigation error caused by IMU constant errors along the non-rotating axes of IMU rotating frame. RMGSINS and GSINS are simulated under the same simulation conditions so as to verify the advantage of RMGSINS in restraining the IMU constant error. Meanwhile, another simulation is performed to verify the correctness of the designed RMGSINS, when the navigation parameters are calculated by using the GSINS mechanization, the IMU constant errors along the non-rotating axes are artificially set as zero, and the simulation results are called true value. The simulation time is set as 30 h, and the simulation conditions are set as Table 1. The ship sails along the 85°N latitude circle with the velocity of 10 m/s, and the swing maneuver condition is set as (19). The simulation results are shown in Fig. 8-Fig. 10.
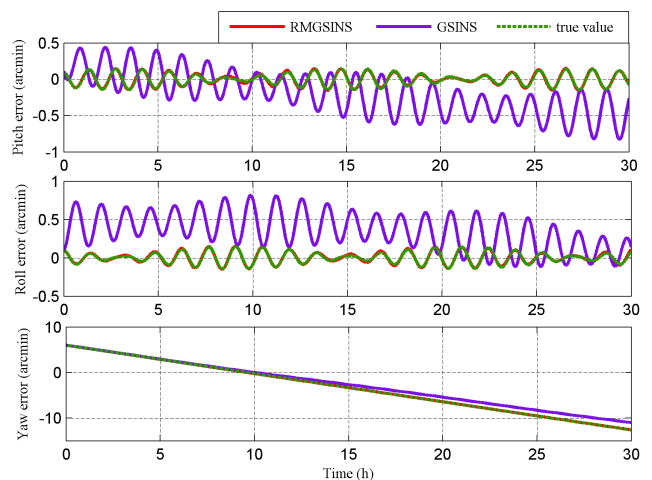

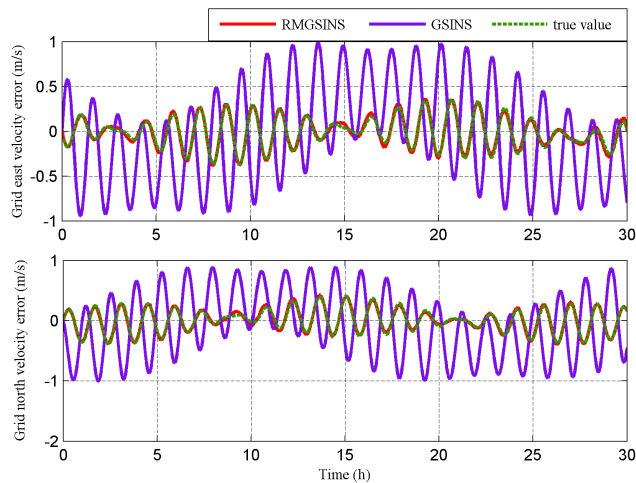**FIGURE 8.** The error curves of the grid attitude angles.

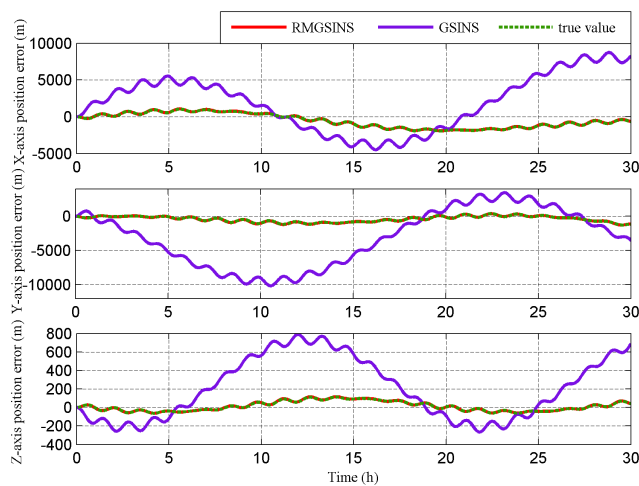**FIGURE 9.** The error curves of the grid horizontal velocities.

FIGURE 10. The position error curves within ECEF frame.

TABLE 2. The RMSs of the attitude errors, velocity errors, and position errors from RMGSINS and GSINS.

Navigation parameter	RMGSINS	GSINS
Pitch (arcmin)	0.0803	0.3538
Roll (arcmin)	0.0713	0.4271
Yaw (arcmin)	6.0192	5.9467
Grid east velocity (m/s)	0.1653	0.5449
Grid north velocity (m/s)	0.1895	0.5511
X-axis position (m)	1.1022×10^3	4.2382×10^3
Y-axis position (m)	0.5940×10^3	5.1445×10^3
Z-axis position (m)	0.0535×10^3	0.3884×10^3
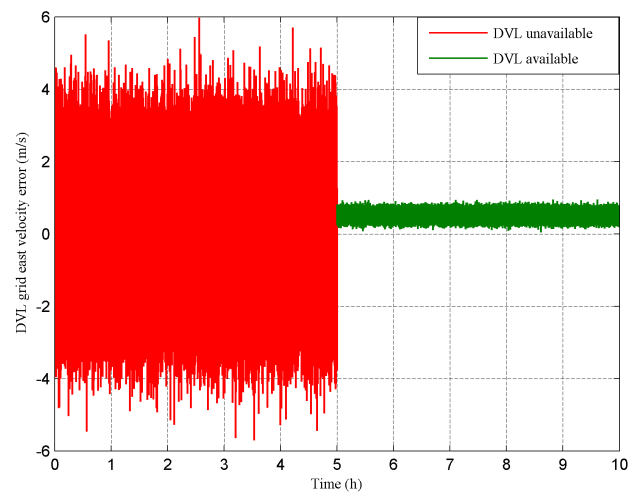
FIGURE 11. The grid east velocity error of DVL.

As shown in Fig. 8-Fig. 10, the solid violet lines and the solid red lines represent the simulation results of GSINS and RMGSINS, respectively; the dotted green lines represent the simulation results of GSINS where IMU constant errors along the non-rotating axes are set as zero. The solid red lines and the dotted green lines coincide with each other, which means the designed RMGSINS has successfully suppressed the navigation error caused by IMU constant errors along the non-rotating axes. Meanwhile, compared with GSINS, because the IMU constant errors along the non-rotating axes have been modulated as the form of periodic change, RMGSINS has smaller navigation error. The root mean-squares (RMSs) of the attitude errors, velocity errors, and position errors are shown in Table 2.

As shown in Table 2, after 30 h, on one hand, the single-axis rotation modulation technique can obviously improve the navigation accuracy of the grid horizontal attitude, the grid horizontal velocity, and the position; on the other hand, because single-axis rotation modulation technique cannot

modulate the IMU constant error along the rotating axis, the grid yaw errors of two schemes are almost same.

After conducting the rotation modulation technique, three kinds of periodical oscillations still exist in RMGSINS, and the IMU random error becomes the leading cause of the navigation error. RMGSINS, T-RMGSINS, and KF-RMGSINS are tested under the same simulation conditions. The simulation time is set as 10 h, and the simulation conditions are set as Table 1. The ship sails along the 85°N latitude circle with the velocity of 10 m/s, and the swing maneuver condition is set as (19). In order to compare the performances of KF-RMGSINS and T-RMGSINS in the process of state switching, the measurement error of DVL is set as follows: before $t = 5\ h$, the measurement error of DVL is set as white noise with large amplitude so as to simulate the condition that the velocity outputted by DVL is unusable, and the system navigates in non-damping state; after $t = 5\ h$, the measurement error of DVL is set as the sum of the constant (1 nmile) and white noise with small amplitude so as to simulate the condition that the velocity outputted by DVL is usable, and the system navigates in horizontal damping state. The grid east velocity error of DVL is shown in Fig. 11.

The simulation results are shown in Fig. 12-Fig. 14.

As shown in Fig. 12-Fig. 14, the dotted red lines, the solid violet lines, and the solid green lines represent
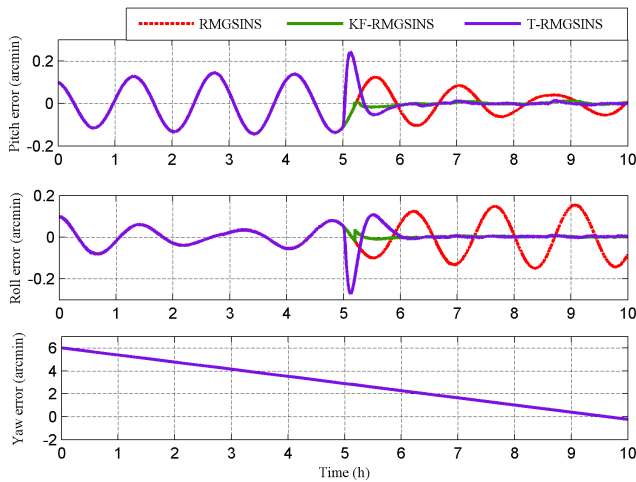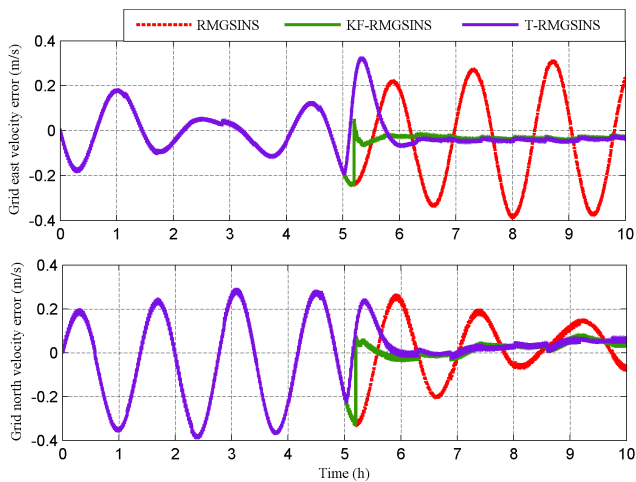
FIGURE 12. The error curves of the grid attitude angles.

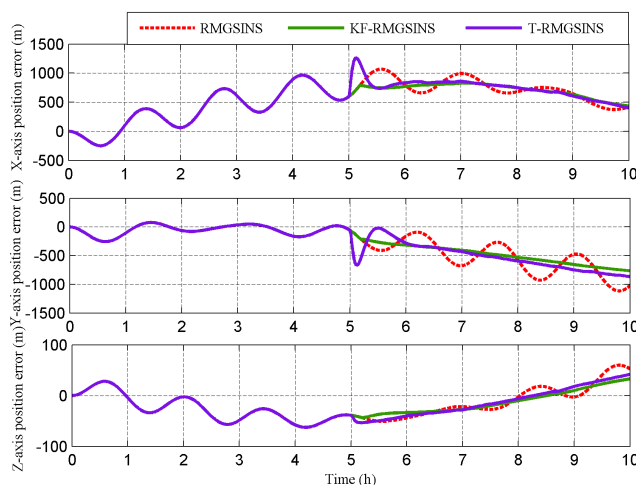**FIGURE 13.** The error curves of the grid horizontal velocities.

FIGURE 14. The position error curves within ECEF frame.

TABLE 3. The RMSs of the attitude errors, velocity errors, and position errors from T-RMGSINS and KF-RMGSINS.

Navigation parameter	T-RMGSINS	KF-RMGSINS
Pitch (arcmin)	0.0012	4.0379×10^{-4}
Roll (arcmin)	0.0014	1.7928×10^{-4}
Yaw (arcmin)	0.0382	0.0382
Grid east velocity (m/s)	0.1304	0.0768
Grid north velocity (m/s)	0.0994	0.0906
X-axis position (m)	8.7027×10^{2}	7.7381×10^{2}
Y-axis position (m)	3.3412×10^{2}	3.1222×10^{2}
Z-axis position (m)	4.1657×10	3.4573×10

and KF-RMGSINS have the same results. After $t = 5$ h, according to the criterion deduced in III-B, the system navigates in horizontal damping state. From the simulation results, T-RMGSINS and KF-RMGSINS both can efficiently damp the Schuler oscillation caused by IMU random error. In order to quantificationally compare the performance of T-RMGSINS and KF-RMGSINS in the process of state switching, the root mean-squares (RMSs) of the attitude errors, velocity errors, and position errors from 5 h-7 h are shown in Table 3. Compared with T-RMGSINS, KF-RMGSINS has the significant advantage of reducing the overshoot errors in the process of state switching. For grid horizontal attitude errors, grid horizontal velocity errors, and position errors, KF-RMGSINS has significant smaller overshoot errors; for grid yaw error, because single-axis rotation modulation technique cannot modulate the IMU constant error along the rotation axis, the grid yaw errors of two schemes are almost same.

B. SEMI-PHYSICAL SIMULATION RESULTS AND DISCUSSIONS

Due to the restriction of acquiring data in polar regions, the semi-physical simulation can be the suitable method to verify the advantage of KF-RMGSINS in practical use. The basic idea of the semi-physical simulation is to add the real IMU measurement noise in low latitude areas to the true IMU measurements in polar regions so as to simulate the real IMU outputs in polar regions. The real measurement noise in low-latitude areas is generated by data collection system in static state, and the true IMU measurement in polar regions is obtained through trajectory generator. The IMU outputs can be expressed as follows:

$$\begin{cases} \boldsymbol{\omega}^b_{ib\_real} = \boldsymbol{\omega}^b_{ib\_true} + \boldsymbol{\varepsilon} \\ \boldsymbol{f}^b_{ib\_real} = \boldsymbol{f}^b_{ib\_true} + \nabla \end{cases} \tag{25}$$

where $\boldsymbol{\omega}^b_{ib\_true}$ and $\boldsymbol{f}^b_{ib\_true}$ represent the theoretical true measurements of the gyroscope and the accelerometer; $\boldsymbol{\omega}^b_{ib\_real}$ and $\boldsymbol{f}^b_{ib\_real}$ represent the measurements of the gyroscope and the accelerometer in practical; $\boldsymbol{\varepsilon}$ represents the gyroscope drift, and ∇ represents the accelerometer bias. When the attitude, the velocity, and the position of the ship are predetermined, the theoretical true measurement of IMU can
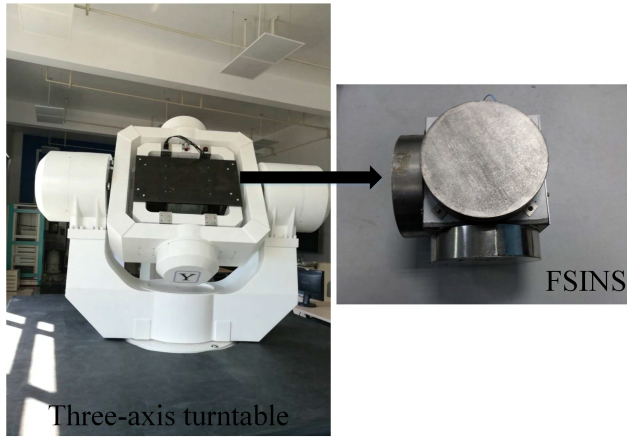
the simulation results of RMGSINS, T-RMGSINS, and KF-RMGSINS, respectively. Before $t = 5$ h, the system works in non-damping state, so RMGSINS, T-RMGSINS,

FIGURE 15. The data collection system in static state.

FIGURE 16. The error curves of the grid attitude angles.

be generated by trajectory generator. In order to get the more realistic IMU outputs, the key is to get the real measurement errors of IMU. The static data collection system to get the real measurement errors of IMU is shown in Fig. 15.

As shown in Fig. 15, the self-made fiber-optic-SINS (FSINS) is installed on the high-precision three-axis turntable. The FSINS is equipped with gyroscopes (drift 0.01 °/h, noise $0.03°/h/\sqrt{Hz}$) and accelerometers (bias 10^{-4}g, noise 10^{-5} g$/\sqrt{Hz}$). The accurate position of the turntable has been determined in the process of installing the turntable, and the position of the static test is 126.67°E and 45.78°N. The turntable can output the accurate attitude reference of FSINS. After the processes of zero adjustment and installation error compensation, the attitude of the FSINS can be approximated to zero, which means the strap-down matrix C_n^b can be approximated to a unit matrix. The main technical parameters of the SGT-8 three-axis turntable are shown in Table 4.

FIGURE 17. The error curves of the grid horizontal velocities.

TABLE 4. The main technical parameters of the SGT-8 three-axis turntable.

	Inner Axis	Middle Axis	Outer Axis
Location accuracy of angular position	±2 arc sec	±2 arc sec	±3 arc sec
Maximum angular rate	±400 °/s	±250 °/s	±180 °/s
Rotation rate resolution	0.001 °/s	0.001 °/s	0.001 °/s

In static test, the three-axis gyroscopes measure the rotational angular velocity of the earth, and the three-axis accelerometers measure the local gravitational acceleration. In this way, with the aid of the attitude reference given by turntable, the real measurement error of IMU can be obtained as follows:

$$\begin{cases} \boldsymbol{\varepsilon} = \boldsymbol{\omega}_{ie\_error}^b = \boldsymbol{\omega}_{ie\_real}^b - \boldsymbol{C}_n^b \boldsymbol{\omega}_{ie}^n \\ \boldsymbol{\nabla} = \boldsymbol{f}_{ie\_error}^b = \boldsymbol{f}_{ie\_real}^b - \boldsymbol{C}_n^b \boldsymbol{f}_{ie}^n \end{cases} \quad (26)$$

where $\boldsymbol{\omega}_{ie\_error}^b$ and $\boldsymbol{f}_{ie\_error}^b$ represent the measurement errors of the gyroscope and the accelerometer in static state;
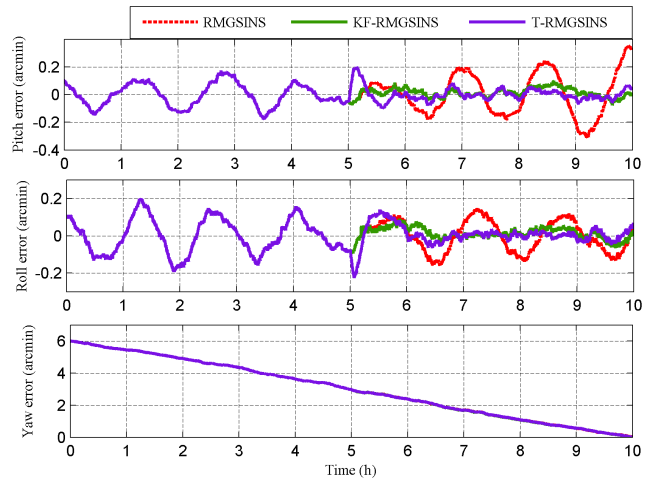
$\boldsymbol{\omega}_{ie\_real}^b$ and $\boldsymbol{f}_{ie\_real}^b$ represent the measurements of the gyroscope and the accelerometer; $\boldsymbol{C}_n^b$ is calculated by using the attitude reference; $\boldsymbol{\omega}_{ie}^n$ is calculated by using the predetermined position information of the turntable; $\boldsymbol{f}_{ie}^n$ is the gravitational gravity within geographic frame. Aiming at RMSINS, the IMU outputs can be generated by using (11).

RMGSINS, T-RMGSINS, and KF-RMGSINS are tested under the same simulation conditions. The simulation time is set as 10 h. The theoretical true measurement of IMU is generated by trajectory generator, and the measurement error of IMU is generated by the static data collection system. The other simulation conditions are set as Table 1. The ship sails along the 85°N latitude circle with the velocity of 10 m/s; and the swing maneuver condition of the ship is set as (19). The measurement error of DVL is set as Fig. 11. The semi-physical simulation results are shown in Fig. 16-Fig. 18:

As shown in Fig. 16-Fig. 18, the dotted red lines, the solid violet lines, and the solid green lines represent
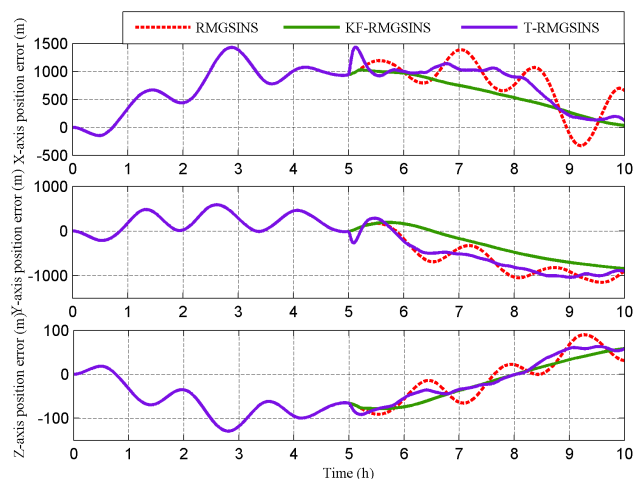
FIGURE 18. The position error curves within ECEF frame.

TABLE 5. The RMSs of the attitude errors, velocity errors, and position errors from T-RMGSINS and KF-RMGSINS.

Navigation parameter	T-RMGSINS	KF-RMGSINS
Pitch (arcmin)	0.0012	9.3314×10^{-4}
Roll (arcmin)	0.0014	9.0563×10^{-4}
Yaw (arcmin)	0.0443	0.0441
Grid east velocity (m/s)	0.2076	0.1178
Grid north velocity (m/s)	0.1769	0.1048
X-axis position (m)	1.3637×10^{3}	1.0841×10^{3}
Y-axis position (m)	1.1167×10^{3}	7.4257×10^{2}
Z-axis position (m)	8.0616×10	7.7999×10

the semi-simulation results of RMGSINS, T-RMGSINS, and KF-RMGSINS, respectively. In order to quantificationally compare the performance of T-RMGSINS and KF-RMGSINS in the process of state switching, the root mean-squares (RMSs) of the attitude errors, velocity errors, and position errors from 5 h-7 h are shown in Table 5. Because the statistic of process noise in semi-physical simulation is more complex than that of pure simulation, the results of two simulations have some differences which will not affect the final conclusions. The semi-physical simulation results coincide with the simulation results in general. On one hand, KF-RMGSINS can effectively damp the Schuler oscillation caused by IMU random error; on the other hand, compared with T-RMGSINS, KF-RMGSINS has significant smaller overshoot errors in the process of state switching except grid yaw error.

V. CONCLUSION

The single-axis rotation modulation scheme is conducted to restrain the navigation error caused by IMU constant error. The simulation results demonstrate that the designed RMGSINS can effectively eliminate the navigation error caused by IMU constant error. In order to further improve the navigation accuracy of the ship sailing in polar regions,

a novel external horizontal damping algorithm named KF-RMGSINS is conducted to suppress the navigation error caused by IMU random error. The simulation results demonstrate that compared with T-RMGSINS, KF-RMGSINS can suppress the Schuler oscillation caused by IMU random error efficiently, meanwhile it has the advantage of reducing the overshoot errors when the system state switches from non-damping state to damping state. The advantage of KF-RMGSINS effectively improves the navigation accuracy in the process of state switching, which makes the navigation information keeps valid for a long time.
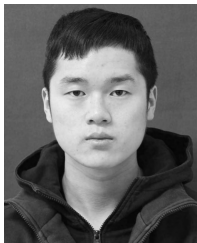
REFERENCES
[1] J. Cheng, T. Wang, D. Guan, and M. Li, "Polar transfer alignment of shipborne SINS with a large misalignment angle," *Meas. Sci. Technol.*, vol. 27, no. 3, p. 035101, Jan. 2016.

[2] L. Paull, S. Saeedi, M. Seto, and H. Li, "AUV navigation and localization: A review," *IEEE J. Ocean. Eng.*, vol. 39, no. 1, pp. 131–149, Jan. 2014.

[3] L. Guo, S. Cao, C. Qi, and X. Gao, "Initial alignment for nonlinear inertial navigation systems with multiple disturbances based on enhanced anti-disturbance filtering," *Int. J. Control*, vol. 85, no. 5, pp. 491–501, 2012.

[4] T. Wang, J. Cheng, D. Guan, Y. Kang, and W. Zhang, "Modified compensation algorithm of lever-arm effect and flexural deformation for polar shipborne transfer alignment based on improved adaptive Kalman filter," *Meas. Sci. Technol.*, vol. 28, no. 9, p. 095101, Aug. 2017.

[5] E. W. Anderson, "I—Navigation in polar regions," *J. Navigat.*, vol. 10, no. 2, pp. 156–161, Apr. 1957.

[6] E. Levinson, J. T. Horst, and M. Willcocks, "The next generation marine inertial navigator is here now," in *Proc. IEEE/ION PLANS*, Las Vegas, NV, USA, Aug. 1994, pp. 121–127.

[7] Q. Zhou, Y. Qin, Q. Fu, and Y. Yue, "Grid mechanization in inertial navigation systems for transpolar aircraft," *J. Northwestern Polytechnical Univ.*, vol. 31, no. 2, pp. 210–217, Apr. 2013.

[8] F. Wu, Y. Qin, and Q. Zhou, "Airborne weapon transfer alignment algorithm in polar regions," *J. Chin. Inertial Technol.*, vol. 21, no. 2, pp. 141–146 and 158, Apr. 2013.

[9] Q. Li, Y. Ben, F. Yu, and F. Sun, "System reset of transversal strapdown INS for ship in polar region," *Measurement*, vol. 60, pp. 247–257, Jan. 2015.

[10] Y.-Q. Yao, X.-S. Xu, Y. Li, Y.-T. Liu, J. Sun, and J.-W. Tong, "Transverse Navigation under the Ellipsoidal Earth Model and its Performance in both Polar and Non-polar areas," *J. Navigat.*, vol. 69, no. 2, pp. 335–352, Mar. 2016.

[11] Q. Zhou, Y.-Z. Yue, X.-D. Zhang, and Y. Tian, "Indirect grid inertial navigation mechanization for transpolar aircraft," *J. Chin. Inertial Technol.*, vol. 22, no. 1, pp. 18–22 and 66, Feb. 2014.

[12] K. R. Greenaway and M. D. Gates, *Polar Air Navigation: A Record*. Winnipeg, Canada: Art Bookbindery, 2009, pp. 53–126.

[13] Z. Yan, L. Wang, W. Zhang, J. Zhou, and M. Wang, "Polar grid navigation algorithm for unmanned underwater vehicles," *Sensors*, vol. 17, no. 7, p. 1599, Jul. 2017.

[14] G.-D. Zhang, G- M. Yan, J. Weng, and H.-T. Yang, "N-vector inertial navigation mechanization algorithm for transpolar aircraft," *J. Chin. Inertial Technol.*, vol. 25, no. 5, pp. 606–610 and 617, Oct. 2017.

[15] Y. Kang, L. Zhao, J. Cheng, M. Wu, and X. Fan, "A novel grid SINS/DVL integrated navigation algorithm for marine application," *Sensors*, vol. 18, no. 2, p. 364, Jan. 2018.

[16] N. Aboelmagd, T. B. Karamat, and J. Georgy, *Fundamentals of Inertial Navigation, Satellite-based Positioning and Their Integration*. Berlin, Germany: Springer-Verlag, 2013, pp. 125–166.

[17] S. Ishibashi, T. Aoki, I. Yamamoto, S. Tsukioka, H. Yoshida, and T. Hyakudom, "The method to improve the performance of an inertial navigation system using a turntable," in *Proc. ISPE*, San Francisco, CA, USA, 2006, pp. 229–232.

[18] Y. Jia, S. Li, Y. Qin, and R. Cheng, "Error analysis and compensation of MEMS rotation modulation inertial navigation system," *IEEE Sensors J.*, vol. 18, no. 5, pp. 2023–2030, Mar. 2018.

[19] P.-M. Lee, B.-H. Jun, K. Kim, J. Lee, T. Aoki, and T. Hyakudome, "Simulation of an inertial acoustic navigation system with range aiding for an autonomous underwater vehicle," *IEEE J. Ocean. Eng.*, vol. 32, no. 2, pp. 327–345, Apr. 2007.

[20] Q. Li, F. Sun, Y.-Y. Ben, and F. Yu, "Transversal strapdown INS and damping design in polar region," *Syst. Eng. Electron.*, vol. 36, no. 12, pp. 2496–2503, Dec. 2014.

[21] W. Huang, T. Fang, L. Luo, L. Zhao, and F. Che, "A damping grid strapdown inertial navigation system based on a Kalman filter for ships in polar regions," *Sensors*, vol. 17, no. 7, p. 1551, Jul. 2017.

[22] J. Sun, X. Xu, Y. T. Liu, T. Zhang, Y. Li, and J. Tong, "An adaptive damping network designed for strapdown fiber optic gyrocompass system for ships," *Sensors*, vol. 17, no. 3, p. 494, Mar. 2017.

[23] K. R. Britting, *Inertial Navigation Systems Analysis*. Norwood, MA, USA: Artech House, 2010, pp. 226–260.

[24] W. Gao, Y. Zhang, Y. Ben, and Q. Sun, "An automatic compensation method for states switch of strapdown inertial navigation system," in *Proc. IEEE/ION PLANS*, Myrtle Beach, SC, USA, Apr. 2012, pp. 814–817.

[25] L. Zhao, J. Li, J. Cheng, and Y. Hao, "Damping strapdown inertial navigation system based on a Kalman filter," *Meas. Sci. Technol.*, vol. 27, no. 11, p. 115102, Sep. 2016.

[26] H. Hongyang, X. Jiangning, Q. Fangjun, and Z. Feng, "Research on generalized inertial navigation system damping technology based on dual-model mean," *Proc. Inst. Mech. Eng., G, J. Aerosp. Eng.*, vol. 230, no. 8, pp. 1518–1527, Jun. 2016.

[27] Q. Y. Yuan, *Inertial Navigation*. Beijing, China: Science Press, 2014, pp. 194–356.

[28] X. Wang, J. Wu, T. Xu, and W. Wang, "Analysis and verification of rotation modulation effects on inertial navigation system based on MEMS sensors," *J. Navigat.*, vol. 66, no. 5, pp. 751–772, 2013.

WEIQUAN HUANG received the B.S. degree in underwater acoustic electronics from the Harbin Shipbuilding Engineering Institute, in 1989, and the M.S. degree in information and signal processing and the Ph.D. degree in control theory and control engineering from Harbin Engineering University, in 1994 and 2006, respectively, where he is currently a Professor with the College of Automation. His current research interests include underwater navigation, integrated navigation technology and new inertial devices, and high-precision navigation systems.

TAO FANG received the B.S. degree from the School of Electrical and Control Engineering, North University of China, Taiyuan, China, in 2014. He is currently pursuing the Ph.D. degree in control science and engineering with the College of Automation, Harbin Engineering University, Harbin, China. His current research interests include polar navigation, information fusion, and its application in integrated navigation systems.

LI LUO received the B.S. and M.S. degrees from the College of Automation, Harbin Engineering University, Harbin, China, in 2015 and 2017, respectively, where she is currently pursuing the Ph.D. degree in control science and engineering. Her current research interests include information fusion and its application in integrated navigation systems.

• • •